



RAMAN MAPPING SPECTROSCOPY AND GRAVIMETRIC STUDIES ON CORROSION INHIBITION OF CARBON STEEL IN HYDROCHLORIC ACID SOLUTION WITH *MENTHA PULEGIUM* ESSENTIAL OIL

Nadia BELARBI,^{a,b} Naziha CHABANE^c and Fayçal DERGAL^{a,c,*}

^a Scientific and Technical Research Center for Physicochemical Analysis (CRAPC), PO Box 384, industrial zone 42004 Tipaza, Algeria

^b Laboratory of Spectrochemistry and Structural Pharmacology, Department of Chemistry, Faculty of Sciences, University of Tlemcen, PO Box 119, 13000 Tlemcen, Algeria

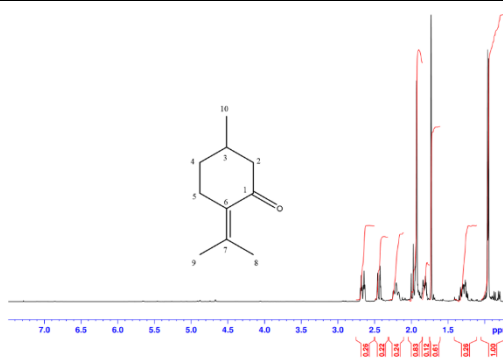
^c Laboratory of Catalysis and Synthesis in Organic Chemistry (LCSCO), Faculty of Sciences, University of Tlemcen, PO Box 119, 13000 Tlemcen, Algeria

Received January 31, 2025

Plant essential oils are among the most promising alternatives to conventional corrosion inhibitors, due to their organic nature, biodegradability, and low toxicity, making them an environmentally friendly option. In this content, the current study focuses on the investigation of the inhibitory efficiency of *Mentha Pulegium* essential oil, predominantly comprising pulegone (74.3%) in protecting carbon steel from corrosion in an aggressive acidic medium, represented by 1M hydrochloric acid (HCl) using a gravimetric method to measure the rates of mass loss resulting from corrosion and Raman spectroscopy to study the surface morphology.

To assess the impact of temperature and oil concentration on inhibition efficiency, tests were performed at 30–60°C with concentrations from 12 to 100 ppm. The synergistic effect of adding a small amount of potassium iodide (0.15%) was also investigated, to determine whether non-metallic particles could enhance inhibition efficiency by improving the adsorption of active compounds to the metal surface. The results showed that *Mentha Pulegium* essential oil exhibited promising inhibitory properties, with the highest inhibition efficiency reaching 63% at a concentration of 100 ppm and a temperature of 30°C. This efficiency increased to 83% after the addition of KI, indicating a synergistic effect resulting from the enhanced adsorption of organic molecules to the steel surface by iodide ions. The surface morphology of the steel after inhibition, confirms the formation of a smooth and stable protective layer compared to the untreated surface. Adsorption data showed good agreement with the Langmuir model, indicating that inhibition is primarily driven by a physical adsorption mechanism. Thermodynamic analyses also supported this conclusion, with ΔG^0 values falling within the range associated with physical adsorption.

This study highlights the high effectiveness of *Mentha Pulegium* essential oil as a natural corrosion inhibitor, either alone or in synergistic combination with potassium iodide, opening up broad prospects for its use as a "green" inhibitor in corrosion protection applications in the chemical and petrochemical industries, particularly in aggressive acidic environments.



INTRODUCTION

Metals like steel are an integral part of our lives given the many areas they cover. They have excellent

mechanical properties,¹ are abundant, easy to recycle and relatively inexpensive. Unfortunately, they are not very resistant to abrasion from environmental conditions (humidity, oxygen, acid rain, etc.) and

* Corresponding author: dergalf@yahoo.fr

operating conditions such as contact with corrosive compounds like acids.²

Acid solutions are widely used in industry, the main fields of application are acid pickling or cleaning, stimulation of oil wells and removal of local deposits (non-uniformly distributed scale, rust, bacterial deposits, etc.).²⁻⁹

Consequently, the problem of corrosion of steel is accompanied by serious problems. However, corrosion can be controlled or significantly slowed by various strategies. The use of inhibitors is one of the most economical and promising approaches.^{4,10-16}

An inhibitor is a compound added in small amounts to the medium to reduce the corrosion rate of the material. It can be used to permanently or temporarily protect parts. Extensive research on these compounds has led to the successful development of specific products or product mixtures corresponding to a given corrosion system. However, each case of corrosion remains a special case, and it is necessary to know the basic operating data of these inhibitors, their limits of use, their particular toxicity, in order to be able to use them with a sufficient margin of safety.

In view of the new environmental constraints, today's challenge is the development of eco-compatible and biodegradable corrosion inhibitors.¹⁶ It is especially for this reason, whereas research is mainly directed towards non-toxic and stable organic molecules called green inhibitors which are the subject of great attention in the world of industry because of their non-toxic properties and efficiency in the field of corrosion.¹⁷⁻²⁰

Natural chemicals derived from plant extracts are regarded as environmentally friendly inhibitors of steel corrosion in various hostile solutions, due to their heteroatoms having numerous bonds.^{4,15,19}

These natural compounds have been used as corrosion inhibitors for many metals in different media, according to multiple studies.^{21-32,33-36} The protection strategy is attributed to adsorption on the steel substrate,¹ thus inhibiting corrosion sites. The protective barrier formed between the corrosive solution and the steel surface is the main deterrent to the steel dissolving in the corrosive environment.^{14,18,37}

Recent advancements in Raman spectroscopy, coupled with mapping techniques, have brought about a paradigm shift in the characterization of metals. Raman spectroscopy, a potent non-destructive analytical method, allows for the extraction of molecular information by probing the vibrational modes of molecules.³⁸ This technique utilizes laser light to excite the molecules and analyzes the scattered light, enabling the identification of specific functional groups and

chemical constituents present in different types of metals.

Several studies have employed Raman spectroscopy in Metals analysis.³⁹⁻⁴⁴ These studies underscore the considerable potential of Raman spectroscopy and mapping techniques in the comprehensive mechanism of inhibition of corrosion. By offering molecular insights, spatial information, and non-destructive analysis, Raman spectroscopy emerges as a valuable tool for researchers in this field.³⁸⁻⁴⁷

Building on these insights, the present investigation aims to evaluate the effectiveness of *Mentha pulegium* essential oil, known for its medicinal and culinary uses by the Algerian population,⁴⁸ as a natural corrosion inhibitor for carbon steel in an acidic medium of 1M HCl. Particular focus was placed on its main component, pulegone, both alone and in combination with potassium iodide (KI), to test the potential synergistic effect between them using the mass loss method as a quantitative measure of the corrosion rate, along with Raman spectroscopy and mapping to identify distinct spectral signatures corresponding to specific corroded parts for C38 Carbon steel in acidic medium (HCl) with and without the presence of essential oil as an inhibitor. This integrated approach allowed for the spatial visualization of these compounds within the C38 samples, offering valuable insights into their distribution and efficacy of green inhibitor.

EXPERIMENTAL

Materials

The material tested as working electrode is a carbon steel C38 whose chemical composition is: (S: 0,035%, C: 0.30-0.35%, Si: 0.15-0.35%, Mn: 0.05-0.1%, P: 0.035 and Fe balance. The steel samples used are in the form of rectangular plates.

Inhibitors

Mentha Pulegium essential oil

In the present investigation, natural product of *M. Pulegium* plant (MP) is used as corrosion inhibitor for carbon steel. The samples were collected in July 2021 in the province of Maaziz in the north-west of Tlemcen (Algeria). The station's relative GPS coordinates are 34°54'35"N latitude, 1°48'28"W longitude and 526 m the altitude in relation to the sea level. The Aerial part of *M. Pulegium* plant was dried

for two months at ambient temperature before being hydro distilled by a Clevenger-type device for 3 h. Before use, the essential oil was stored at 4°C in sealed glass bottles.

Pulegone

In order to determine the compound(s) responsible for the inhibitory activity of the studied extract, we tested the inhibition effect of the major compound (Pulegone 74.3%) against the corrosion of C38 steel in 1M HCl medium. This investigation should allow us to determine if the inhibition is related to a synergistic effect, addition or competition of all the molecules contained in the oil, or conversely, if this inhibition is only due to the major compound which generally dominates the oil.

The fractionation of the essential oil of *M. Pulegium* was carried out with a chromatography column on silica gel to obtain the pulegone (Fig. 1) using the following eluent: hexane and ethyl acetate (90/10). The chromatography of the oil is performed by diluting four (04) drops of the oil in 1ml of dichloromethane. The same method is performed with pure pulegone. Using a capillary to deposit each sample on a silica plate. After the migration of the eluent the plate is dried then passed to the UV. In silica gel chromatography the migration of the compounds is done by gravity. After the separation, the fractions containing the pulegone were grouped. A proton NMR analysis was performed to confirm the structure of pulegone.

Solutions

The aggressive medium used consisted of a 1M HCl solution prepared from a 37% concentrated solution from Sigma-Aldrich by dilution with distilled water. Five (05) different concentrations 12, 25, 50, 75 and 100 ppm of MP. EO were prepared in 1mol/l concentration of hydrochloric acid.

Concentration of 74.3 ppm of pulegone was also investigated in these media for testing its corrosion inhibition effect alone. This study allows its comparison with the whole extract.

Weight loss measurements

The surfaces of the steel coupons underwent a pre-treatment before each manipulation, which consisted of a mechanical polishing with abrasive paper of increasingly fine granulometry (grade 600-800-1200-2000), in order to obtain a smooth surface, having a mirror-like aspect. Then, the

samples were washed with distilled water, degreased with acetone and rinsed with distilled water, finally dried and stored.

A series of mass loss measurements were performed in a corrosive solution without and with the addition of inhibitor tested over time at different concentrations and temperatures. The steel samples used were immersed vertically for 4h in beakers containing 100ml of the corrosive solution, without and with addition of different concentrations of the inhibitor and at room temperature kept constant at 303 K. At the end of the experiment, the samples were reweighed using an analytical balance. All the aggressive acid solutions were open to air.

An important parameter is the corrosion rate, which is the rate at which a material dissolves as a result of chemical action. It refers to the loss of thickness of a material per unit of time and area.

The corrosion rates of steel samples (W_{corr}) are expressed in $\text{mg}/\text{cm}^2\cdot\text{h}$ and calculated from the following formula:

$$W = \frac{\Delta M}{S \times t} \quad (1)$$

where: ΔM – represents the difference between the initial mass M_1 and the final mass M_2 after a time t equal to 4h; S – sample surface; t – exposure time.

This corrosion rate value is the average of three tests performed under the same conditions for each concentration. The value of the inhibiting efficiency is given by the following formula:

$$E\% = 100 \times \frac{W_0 - W}{W_0} \quad (2)$$

where W_0 , W represent the corrosion rates in the absence and presence of the inhibitor respectively.

Raman spectroscopy

Raman spectroscopic investigation was performed using a HORIBA LABRAM HR Raman spectrometer operated in single spectrograph mode with a holographic dispersive grating of 600 grooves/mm equipped with a frequency (633, 785 and 325 nm).

The samples were analyzed in the back-scattering mode on the microscope stage of an Olympus confocal microscope attached to the spectrometer using a long working distance 50 × objective. The detector used was a liquid nitrogen cooled charge coupled device Symphony IGA detector. A 663 and 785 nm holographic notch filter were used to remove the Rayleigh-scattered light.

The entrance slit width was 100 μm giving a resolution of 2 cm^{-1} in the range between 100 and 5000 cm^{-1} . Repeated acquisition using the highest

magnification were accumulated to improve the signal to noise ratio in the spectra. Spectra were calibrated using the 520.5 cm^{-1} line of a silicon wafer.

Raman experiments were performed with samples of dimension $2.5\text{ cm} \times 2\text{ cm} \times 0.1\text{ cm}$ and were prepared as described above. After immersion in 1.0 M HCl without and with 100ppm of MP.EO at 30°C for 4 h, the specimens were thoroughly washed with distilled water and dried.

RESULTS AND DISCUSSION

Mentha Pulegium oil and pulegone analysis

Mentha Pulegium oil composition

Six volatile compounds that accounted for 94.3% of the total of *Mentha Pulegium* oil were

identified by GC-MS analysis. Pulegone (74.3%) is the major compound followed by p-Cymene (5.4%) and Thymol acetate (5.0%) (Table 1). A study conducted by Fatima Zahra Benomari *et al.*⁴⁹ on the essential oil of the plant *Mentha Pulegium* harvested from three different regions of the wilaya of Tlemcen (Algeria), the study revealed that the chemical composition of the oil differs from one region to another. Region 1: Maaziz (rich in Pulegone (77.3%), Menthone (10.8%) and Neo-Menthol (2.7%)), Region 2: Ghazaouet (Pulegone (40.7%), Menthone (38.3%) and Neo-Menthol (9.1%)) and Region 3: Djbala (Neo-Menthol (42.3%), Menthone (40.5%) and Pulegone (9.2%)).

The structure of the major compound is shown in the Fig. 1.

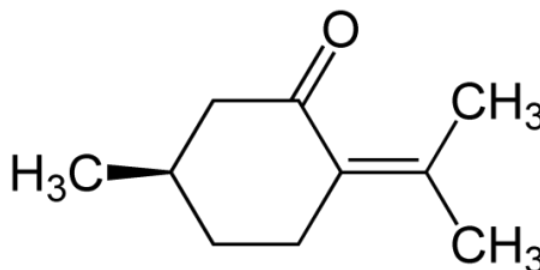


Fig. 1 – Chemical molecular structure of major component in M.P.E.O: Pulegone (74.3%).

Table 1

Chemical composition of *Mentha Pulegium* essential oil

N°	Compounds ^a	RI _a ^b	RI _a ^c	%	Identification
1	p-Cymene	992	961	5.4	RI, MS
2	Cis-p-Menthan-3-one	1159	1041	3.8	RI, MS
3	Trans-p-Menthan-3-one	1142	1042	3.9	RI, MS
4	Pulegone	1244	1085	74.3	RI, MS
5	Thymol	1296	1116	1.9	RI, MS
6	Thymol acetate	1362	1205	5.0	RI, MS
Total identification (%)				94.3%	

^a Order of elution are given on the apolar (HP-5MS) column.

^b Retention indices of literature on the apolar column (RI_a) reported from the literature.

RI^c: Retention Indices.

MS: Mass Spectrometry in electronic impact mode.

¹H NMR of pulegone

The proton NMR spectrum of pulegone was recorded on a Bruker 400 MHz spectrometer.

Manipulation was carried out at 25°C using CDCl_3 to prepare the pulegone specimen and TMS as an internal standard (Fig. 1). The proton NMR data for pure pulegone⁵⁰ after separation are shown in Table 2.

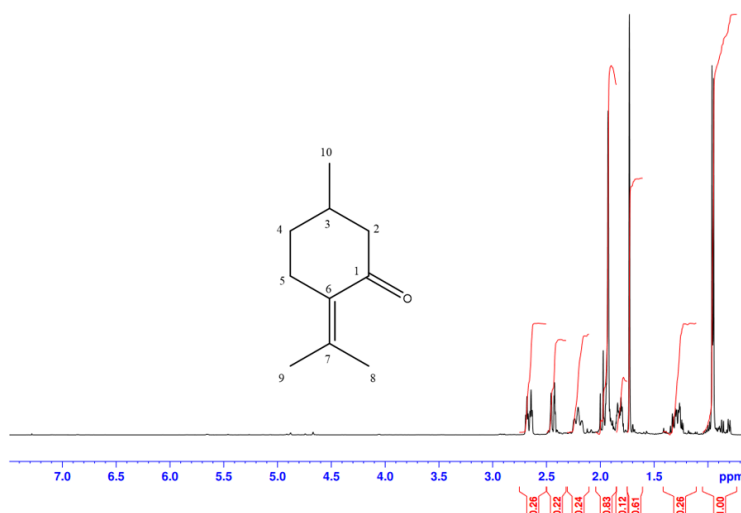
Fig. 2 – ^1H - NMR spectrum of pulegone.

Table 2

The proton NMR data for pulegone.

Carbon	Chemical group	Chemical shifts (ppm)	Multiplicity
2	-CH ₂ -	2.02 and 2.49	m
3	-CH-	1.97	m
4	-CH ₂ -	2.26 and 2.71	m
5	-CH ₂ -	1.31 and 1.87	m
8	=C-CH ₃	1.97	s
9	=C-CH ₃	1.78	s
10	R-CH ₃	1.01	d

Weight loss measurements

Effect of M.P.E.O on corrosion rate

Figure 3 represents the variation of the corrosion rate as a function of the inhibitor concentration in a 1M HCl medium and in a temperature range from 30 to 60°C.

According to this figure, a decrease of the corrosion rate is observed with the increase of the concentration of M.P.E.O, this is probably due to the adsorption of this compound to a higher extent onto the metal surface⁵¹ and the reduction reaction of the hydrochloric acid will be slowed down.

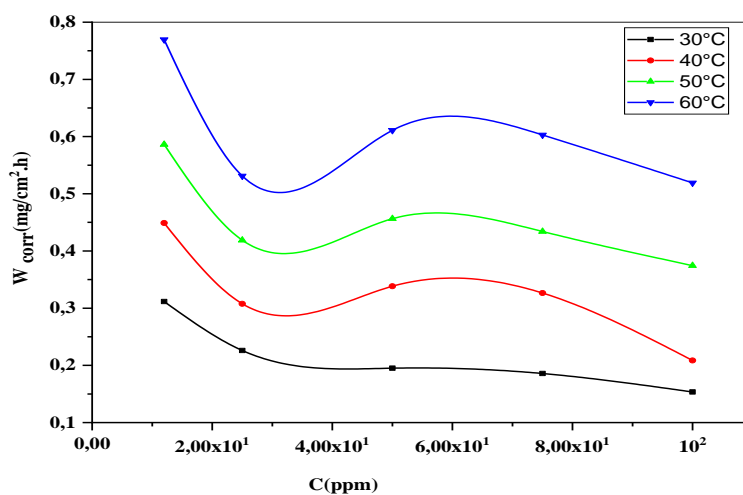


Fig. 3 – Relation of the corrosion rate (W) to the concentration of MP.E.O in 1 M HCl.

Besides, Fig. 3 shows that the corrosion rate in the acidic solution alone (HCl) increases with the increase of the temperature and reaches a rate of $1.0965 \text{ mg/cm}^2 \cdot \text{h}^{-1}$ at 60°C . On the

contrary, the corrosion rate in the case of the inhibitor solution when the temperature rises are clearly very low compared to the case of acid alone.

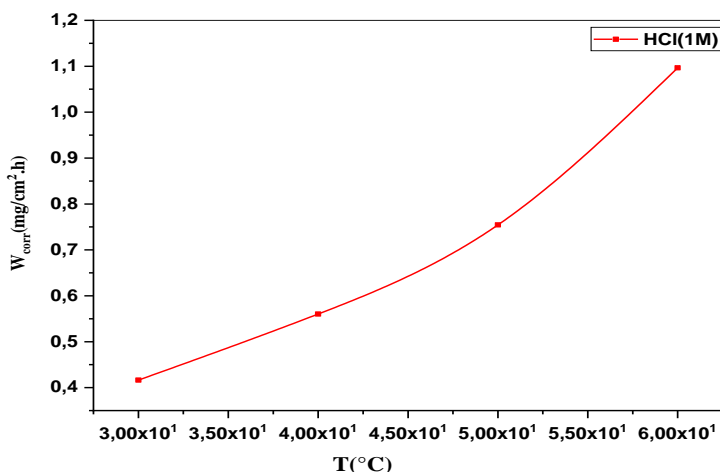


Fig. 4 – Variation of corrosion rate (W) with Temperature for 1 M HCl.

It can be seen that 100 ppm of M.P.E.O inhibitor is sufficient to inhibit the C38 steel corrosion and to slow down the corrosion rate considerably. The concentration of the inhibitor therefore has a significant effect on the corrosion rate which directly affects the inhibitory efficiency.

Effect of M.P.E.O on efficiency inhibition

Results show that the inhibitor concentration has a significant effect on the inhibitory power (Fig. 5) because the inhibition rate increases in parallel with the increase of the inhibitor concentration and reaches a value of 63% at 100 ppm.

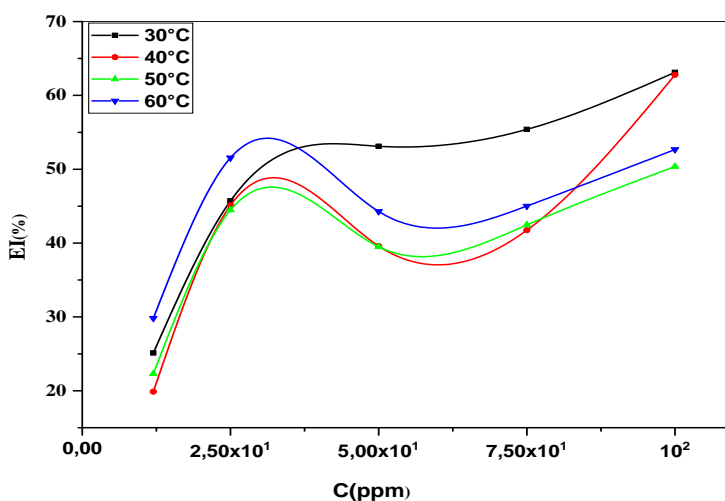


Fig. 5 – Relation of the Efficiency inhibition to the concentration of MP.EO in 1 M HCl.

A further increase in concentration causes no appreciable change in performance. We can say that 100 ppm is the optimum concentration.

The increase in the inhibitory efficiency of M.P.E.O with concentration results from the interaction between

the inhibitor molecules and the metal surface, the inhibitor molecules adsorb on the metal surface and form a protective layer against corrosion.¹⁸

The variation of the inhibiting power as a function of temperature is also shown in Fig. 5.

We observed a decrease in inhibitory efficiency with increasing temperature from 30 to 50°C, while a slight increase is observed at the highest temperature 60°C.

According to OGUZIE *et al.*^{52,53} a decrease in inhibition efficiency with rise in temperature suggests that inhibitor molecules are physically adsorbed on the metal surface, while the reverse behavior suggests chemisorption. Thus, the results

imply that the adsorption of M.P.E.O is mainly the physical adsorption.

Effect of addition of KI to Mentha Pulegium essential oil to corrosion media:

Figure 6 represents the variation of the corrosion rate as a function of the concentration of the inhibitor.

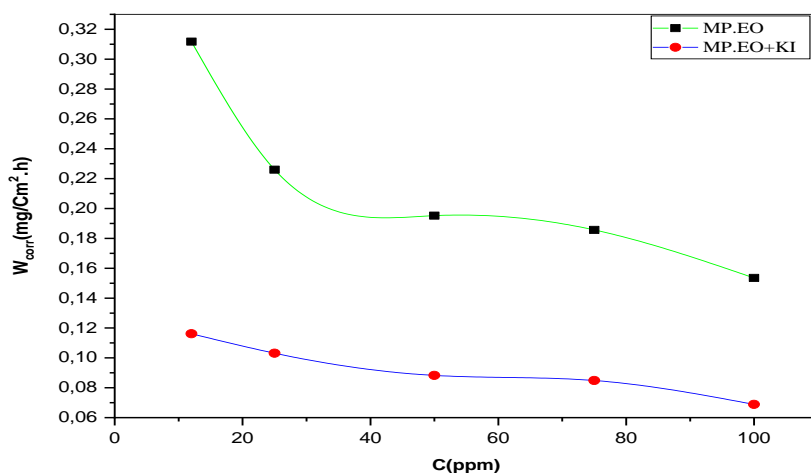


Fig. 6 – Variation of corrosion rate (W) with concentration for *M.P.E.O* and *M.P.E.O+KI*.

As shown in this figure, the addition of KI to M.P.E.O reduced the weight loss of the carbon sheets in the HCl medium. While a weight loss of 0.1535 mg/cm².h was recorded using 100 ppm M.P.E.O, weight loss decreased to 0.0689 mg/cm².h after addition of KI at the same temperature 30°C.

The same applies to all the concentrations examined. In 1 M HCl, M.P.E.O alone gave an

inhibition efficiency of 63%, while the insertion of KI in *Mentha Pulegium* essential oil increased the inhibition efficiency to 83%. The inhibitory power of the mixture was found to be 83% at the highest concentration (100 ppm M.P.E.O + 0.15% KI) more efficient than at the lowest concentration (12 ppm + 0.15% KI) 72%. The observation results clearly show that the addition of KI improved the corrosion inhibition power of M.P.E.O.

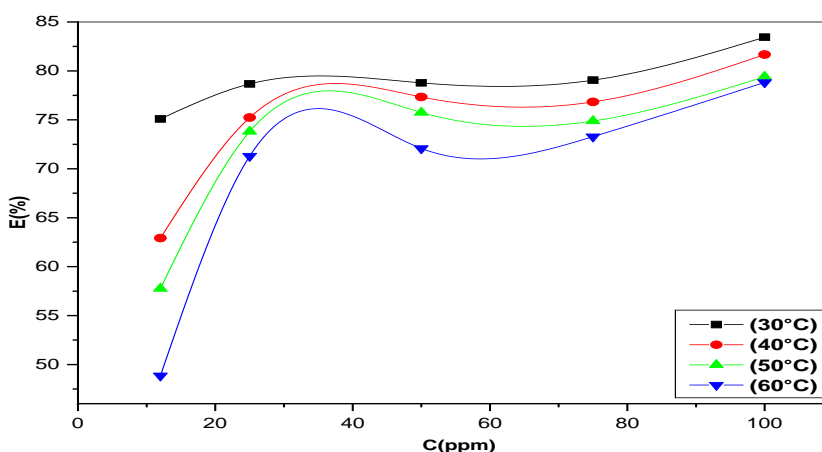


Fig. 7 – Relation of the Efficiency inhibition to the concentration of *M.P.E.O +KI* in 1 M HCl.

We also note that by adding KI to the different concentrations of *Mentha Pulegium* essential oil and at different temperatures, the inhibitory effect decreases with the increase in temperature. For example, for a 0.15% KI + 100 ppm M.P.E.O mixture, the inhibition efficiency was 83% at 30°C, 81% at 40°C, 79% at 50°C and 78% at 60°C.

Thermodynamic activation Parameters

The Arrhenius equation allows taking into account the effect of temperature (T) on the

corrosion rate and thus to consider that the logarithm of the corrosion rate W_{corr} is a linear function of T^{-1} (Eq. 1):

$$\ln(w) = (-E_a/RT) + A \quad (3)$$

where: W – represents the corrosion rate calculated from the gravimetric measurements; A – represents the Arrhenius frequency factor; R – represents the molar gas constant and T – represents the absolute temperature.

Figures 7 and 8 show the Arrhenius coordinate plot of the corrosion rate of steel in 1M HCl in the presence of inhibitor alone and inhibitor+KI.

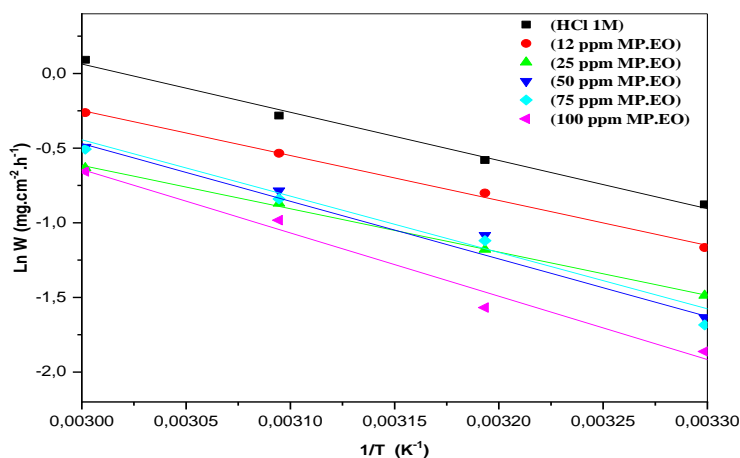


Fig. 8 – $\ln W_{\text{corr}}$ vs $1/T$ for steel in 1M HCl in the absence and presence of M.P.E.O.

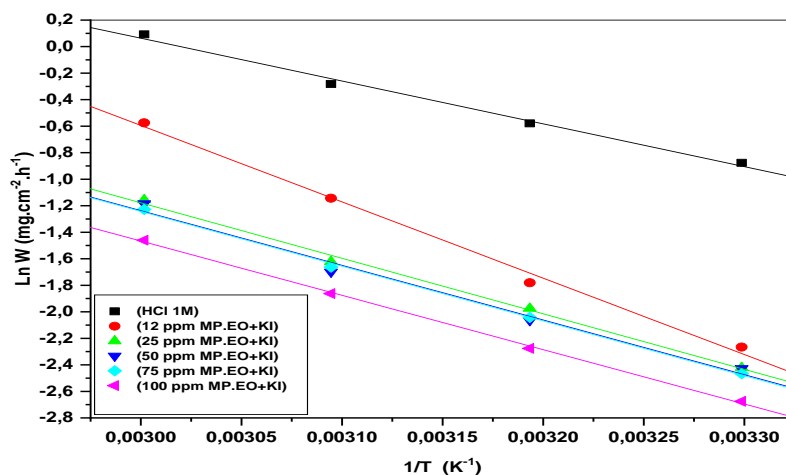


Fig. 9 – $\ln W_{\text{corr}}$ vs $1/T$ for steel in 1M HCl in absence and presence of M.P.E.O + 0.15% of KI.

From these figures, we notice that the curves $\ln W_{\text{corr}} = f(1/T)$ give straight lines, so they follow the Arrhenius law. We can therefore calculate the activation energies from the Arrhenius relation. The activation energies for the different concentrations

without and with the addition of inhibitors are given in Table 3.

An alternative formula of the Arrhenius equation (1) allows to determine the enthalpy and

entropy of activation according to the following equation:¹⁶

$$W = \frac{RT}{Nh} \exp\left(\frac{\Delta S_a}{R}\right) \exp\left(-\frac{\Delta H_a}{RT}\right) \quad (4)$$

where h is Planck's constant; N is Avogadro's number, ΔH_a° is the change in activation enthalpy et ΔS_a° is the change in activation entropy.

The variation of $\ln(W/T)$ as a function of the inverse of temperature is a straight line (Figs. 3 and 4) with a slope of $(-\Delta H_a^\circ / R)$ and an intercept equal to $(\ln R / Nh + \Delta S_a^\circ / R)$.

Therefore, we can calculate the values of ΔH_a° and ΔS_a° . The values of enthalpies and entropies are given in the table below:

Table 3

Activation energy of steel corrosion in the presence of M.P.E.O and MP.EO+KI in HCl 1 M

Inhibitor Concentration	Ea kJ/mol		ΔH_a° (KJ/mol)		$-\Delta S_a^\circ$ (J /mol)	
	MP.EO	MP.EO+KI	MP.EO	MP.EO+KI	MP.EO	MP.EO+KI
0	26,84	26,84	24,19	24,19	172,71	172,71
12ppm	25,04	47,87	22,40	45,23	180,69	115,08
25ppm	24,13	34,80	21,50	32,17	186,46	159,12
50ppm	31,37	34,28	26,08	31,64	163,33	161,18
75ppm	32,11	34,35	29,52	31,71	161,15	161,02
100ppm	35,26	34,05	33,86	31,41	149,31	163,77

From these results, we can draw information on the mechanism of corrosion inhibition of carbon steel.

The calculations show that the activation energy values in the presence of inhibitors were higher than that of the blank solution. This observation implies that the adsorption was by physisorption.⁵⁴⁻⁵⁸

This increase in the activation energy value could be attributed to a significant increase in the energy barrier, confirming the formation of a complex compound at the inhibitor-carbon steel interface.⁵⁶

The positive enthalpy signs reflect the endothermic nature of the dissolution process of carbon steel,^{15,16,59} the increase in adsorption enthalpy in the presence of the additives corresponds to a decrease in metal dissolution.⁶⁰

The negative value of the standard entropy reflects a decrease in the disorder that occurs during the formation of the metal/adsorbed molecule complex.¹⁵

Adsorption isotherm

The inhibition of metal corrosion by organic compounds is explained by their adsorption on the metal surface. The adsorption isotherms are then an

important complement that can determine the electrochemical mechanism that leads to the adsorption of these organic compounds on the surface. The recovery rates (θ) were used to determine the best isotherm that describes the adsorption process of the studied oil at the chosen temperatures. To identify the type of adsorption corresponding to our study, different types of isotherms were tested: Langmuir, Temkin, Frumkin, Flory Huggins, and Freundlich. The correlation coefficients (R^2) were used to select the most representative isotherm. Analysis of the results shows that the adsorption of the inhibitor molecules (MP.EO alone and MP.EO+KI) on the steel surface in 1M HCl medium obeys the Langmuir adsorption isotherm. Therefore, the corrosion inhibition is due to the formation of a monolayer on the metal surface, limiting the access of the electrolyte. The correlation coefficients (R^2) are all close to 1 (>0.99) for both cases, confirming the validity of the model. The Langmuir model assumes that the interactions between the adsorbed particles are negligible and, therefore, the adsorption energy is considered as constant. With these assumptions, and for a given temperature, the relationship between the adsorbed quantity of a species and its concentration in the liquid phase in contact with the

surface is given by the following equation:^{61,62}

$$\frac{C_{inh}}{\theta} = \frac{1}{K_{ads}} + C_{inh} \quad (5)$$

where: C is the concentration of the inhibitor in the electrolyte, K_{ads} the equilibrium constant of the adsorption process.

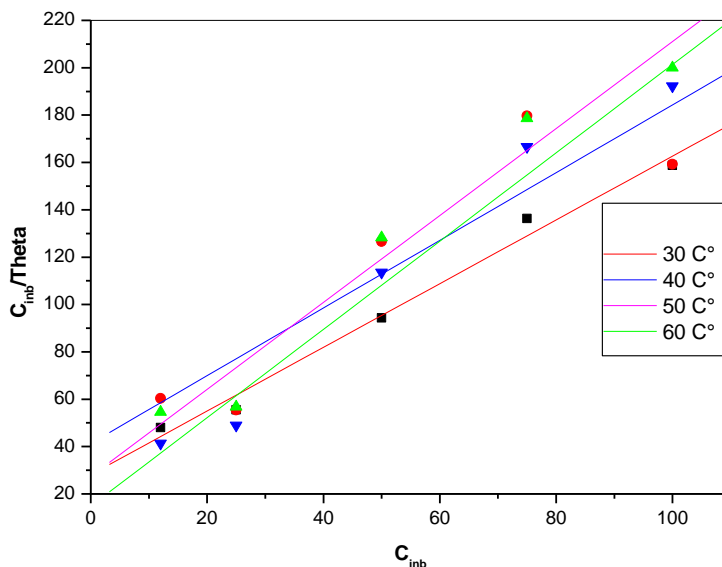


Fig. 10 – Langmuir adsorption isotherm for carbon steel immersed in 1M hydrochloric acid with addition of MP.EO at different temperatures.

Plotting C/θ as a function of the concentration of the essential oil for each case gives

a linear line (Figs. 10, 11), these lines give the $1/K$ values and from these the K values are deduced.

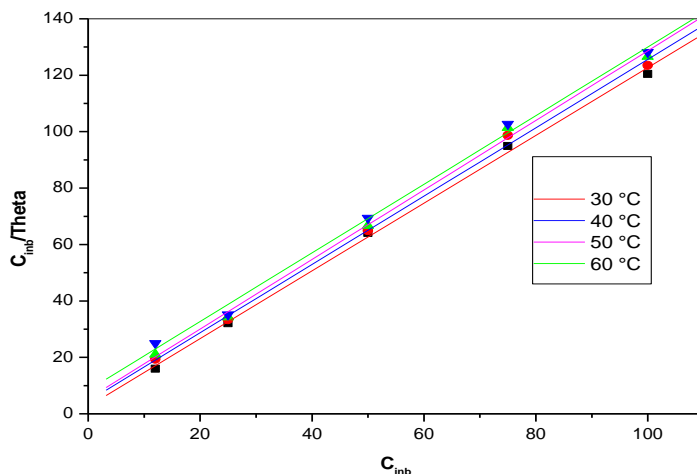


Fig. 11 – Langmuir adsorption isotherm for carbon steel immersed in 1M hydrochloric acid with addition of (M.P.E.O+K.I) at different temperatures.

K_{ads} is related to the standard free energy of adsorption (ΔG_{ads}) by the following relationship:

$$K_{ads} = \frac{1}{C(sol)} \exp\left(-\frac{\Delta G_{ads}}{RT}\right) \quad (6)$$

The standard free energy of adsorption (ΔG_{ads}) can therefore be calculated:

$$\Delta G_{ads}^{\circ} = -RT \ln(K_{ads} \times 55.5) \quad (7)$$

where:

R is the perfect gas constant ($8.314 \text{ J}\cdot\text{mol}^{-1}\cdot\text{K}^{-1}$); T is the absolute temperature, and the value 55.5 is the concentration of water in solution expressed in M .

From the adsorption coefficient (K) obtained the free energy of adsorption (ΔG_{ads}) was calculated and is presented in Table 3.

Generally, for values of adsorption ΔG_{ads} around $-20 \text{ KJ}\cdot\text{mol}^{-1}$, the type of adsorption is considered as physisorption; those around $-40 \text{ KJ}\cdot\text{mol}^{-1}$ or more negative are associated with chemisorption.^{16,58,63-66}

The negative ΔG_{ads} values for the studied systems imply that the adsorption of the inhibitors on the carbon steel surface was spontaneous, and the adsorbed film on the metal surface is stable.

Table 4

Adsorption energy values (ΔG_{ads}) of steel corrosion in the presence of M.P.E.O and M.P.E.O + KI in HCl 1 M

Temperature	ΔG_{ads} (kJ/mol) M.P.E.O	ΔG_{ads} (kJ/mol) M.P.E.O +KI
30 °C	-26,4	-32 ,4
40 °C	-26,26	-32,04
50 °C	-28,21	-32,57
60 °C	-30,77	-32,36

The ΔG_{ads}° values obtained in both cases suggest that M.P.E.O and M.P.E.O + KI are physisorbed on the metal surface, resulting in electrostatic interactions between the metal surface and the formed film. The increase in ΔG_{ads}° values in the presence of KI indicates a stronger interaction of the inhibitor molecules with the metal surface in the presence of KI.

Synergism parameter

To explore the synergistic inhibition that was measured by using the surface coverage values (Θ) of the anion, cation, and both, a metric known as synergistic (SP) was utilized. The following equation was utilized in the determination of SP:^{67,68}

$$SP = (1 - P_{1+2}) / (1 - P'_{1+2}) \quad (8)$$

$$P_{1+2} = (P_1 + P_2) - (P_1 * P_2) \quad (9)$$

P_1 represents the surface coverage of KI, P_2 represents the surface coverage of MP, and P'_{1+2} represents the surface coverage of KI and MP blend.

In case of $SP = 1$, it means that the MP and KI have no effect on each other and they absorb on the metal surface independently (no interaction between MP and KI). In case of $SP < 1$, antagonistic behavior prevails due to a competitive adsorption. While at $SP > 1$, a synergistic effect is obtained as a result of a co-operative adsorption.⁵⁶

In other words, co-operative adsorption (also known as a synergistic effect), in which the anion is chemisorbed on the metal surface, followed by the adsorption of the cation on an anion layer, as opposed to competitive adsorption (also known as an antagonistic effect), in which the anion and cation are adsorbed at different sites on the metal surface. Figure 8 shows that the values of SP for all investigated concentrations of M.P.E.O with 0.15% KI were less than one and decreased with inhibitor concentration, indicating that the improved inhibitory efficacy was caused by the adsorption of iodide ions and MP at separate locations on the surface of the steel. Co-adsorption, also known as competitive adsorption, happens when the iodide anion and the inhibitor (MP) are adsorbed at separate locations on the metal's surface.⁶⁹

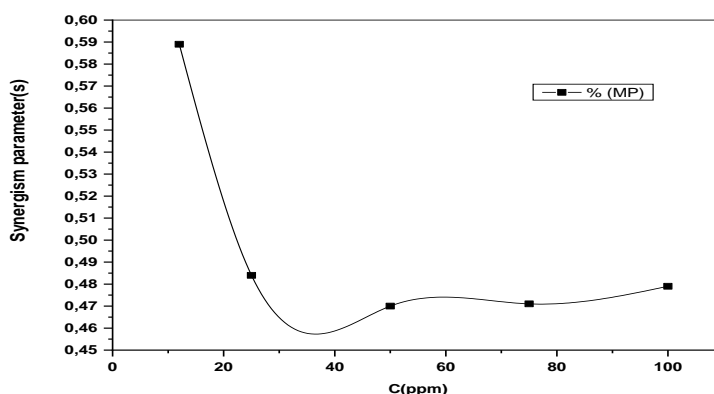


Fig. 12 – The relationship between synergism parameter (SP) and the concentration of inhibitor (C) in the presence of 0.15% KI in 1 M HCl solution at 30°C.

Effect of major component

Gravimetric tests performed revealed that the dominant compound showed an inhibitory efficiency of 65% at 74.3ppm, almost similar to the starting crude oil 63%, as it can be seen from Fig.13.

Thus, we can say that the effectiveness of M.P.E.O may be attributed to the coverage of carbon steel surface with M.P.E.O major compound.⁷⁰

The presence of ketones groups in the molecular structure of the major compounds

significantly aids in inhibiting the corrosion of carbon steel.⁷¹ It's adsorption onto the carbon steel surface through nonbonding electron pairs of oxygen atoms as well as π -electrons block the active sites on carbon steel, and thus, reducing the corrosion rate.⁷² The better protection of the essential oil implies a higher binding capacity of these molecules on the surface of carbon steel surface.

Also, we notice that the addition of KI (0.15%) significantly increases the inhibitory efficiency of pulegone (from 65% to 80%).

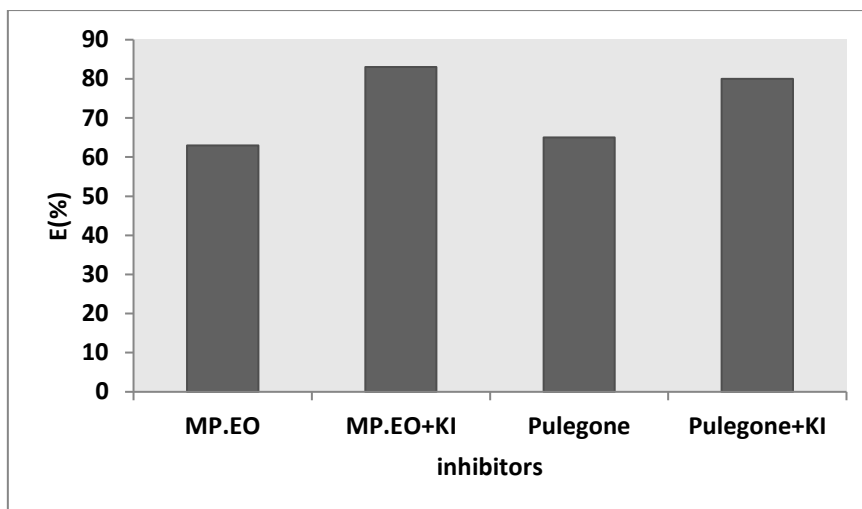


Fig. 13 – Values of the corrosion-inhibiting effectiveness of steel in 1M HCl after addition of: M.P.EO, MP+KI, pulegone and pulegone +KI.Raman Analysis.

The Raman Electronic Microscopy (Fig. 14) of the surfaces of C38 Steel samples were taken at same magnification to see the changes that occurred

during corrosion process in the absence and presence of essential oil at 1M HCl during 4 h at 30°C.

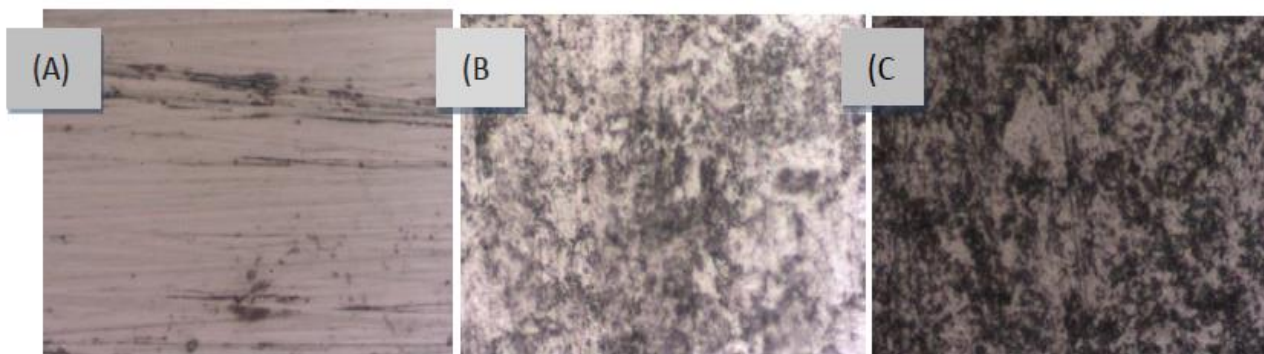


Fig. 14 – Raman Electronical microscopy morphologies of: (A) Carbon steel C38, (B) in 1 M HCL and (C) 1 M HCl + 100 ppm *Mentha Pulegium* Essential Oil for 4 h immersion (magnification $\times 100$).

The electron microscopy (EM) images provide insightful observations regarding the Carbon Steel plate C38 under various conditions. Without the

inhibitor (Fig. 14B), the surface manifests irregularities and damage, indicative of an accelerated corrosion attack when juxtaposed with

the pristine Carbon Steel plate C38 (Fig. 14A). In contrast, the presence of the inhibitor (Fig. 14C) results in a smoother and less corroded surface morphology for Carbon Steel plate C38.

This disparity suggests that the inhibitor's molecules likely adsorb onto the C38 surface, contributing to the suppression of corrosion. The hypothesis is that these inhibitor molecules form an adherent deposit on the C38 surface, thereby restricting electrolyte access and mitigating corrosion. This observation is consistent with the outcomes derived from weight loss measurements, reinforcing the credibility of the findings.

The distinctive morphological variations captured by EM imaging underscore the pivotal role played by the inhibitor in influencing the corrosion behavior of Carbon Steel plate C38. The contrast between the irregular and damaged surface in the absence of the inhibitor and the smoother surface in its presence implies a protective mechanism attributed to the inhibitor's adsorption.

Understanding these surface modifications enhances our comprehension of corrosion dynamics, offering valuable insights for developing effective corrosion inhibition strategies. The results hint at the potential of inhibitors to form protective layers, providing a promising avenue for further exploration in corrosion control methodologies.

Drawing insights from gravimetric measurements, it becomes evident that the corrosion process of C38 steel in a 1 M HCl solution is effectively mitigated in the presence of *Mentha Pulegium* Essential Oil. The discerned outcomes unequivocally point towards an inhibition mechanism primarily driven by the adsorption of inhibitor molecules, leading to the effective blockade of the C38 steel surface. Within the domain of corrosion inhibition expertise, it is firmly established that the efficacy of this adsorption phenomenon is intricately linked to both the inherent nature of the metal and the chemical structure of the inhibitor.

The thermodynamic parameters associated with inhibitor adsorption offer valuable insights into the corrosion inhibition mechanism.^{38,39} The adsorption process of *Mentha Pulegium* Essential Oil on the surface of C38 steel is primarily characterized by physisorption. In this context, the Terpenes, predominantly Pulegone, extracted from *Mentha Pulegium* Essential Oil exhibit an ability to electrostatically adsorb onto the steel surface. Notably, even in an acidic environment, these compounds do not persist as free bases in solution.

Hence, it is reasonable to hypothesize that the initial interaction between the metal surface and the terpenes extract occurs in the protonated form of the compounds. As corrosion initiates, the cationic form may attach itself to the anodic sites. Alternatively, the alkalinity generated at the cathodic sites might revert the compounds to their free base form. Consequently, the adsorption of the terpenes extract onto the metal surface may transpire directly through donor–acceptor interactions, involving the p electrons of the heterocyclic compound and the unoccupied 'd' orbitals of iron surface atoms.^{38,39}

However, a synergistic or antagonistic effect of these molecules may play an important role on the inhibition efficiency of *Mentha Pulegium* Essential Oil. The adsorption of *Mentha Pulegium* Essential Oil on the steel surface is documented from the Raman spectra mapping (Figs. 14 and 15).

M Lebrini *et al.*³⁸ show The Raman spectra obtained that the bands referenced between 1150 and 1610 cm^{-1} were replaced by two large bands centered at 1349 and $\approx 1580 \text{ cm}^{-1}$, indicating a possible chemical change of the *Mentha Pulegium* Essential Oil once adsorbed on the surface. This characteristic peak that we will use as references to make our mappings, these peaks are CH in plane bending; 1380 cm^{-1} and C=C; 1580 cm^{-1} for Aromatic ring.

The first pick at 1380 cm^{-1} will be presented in red to show the corroded part and the second pick at 618 cm^{-1} characteristics of C38 steel (Magnetite)³⁹ on the surface is represented in blue to show C38 Steel non corroded parts.

Figure 14A shows the 3D image of the plate in an acidic 1M HCl medium, where we can notice an irregularity in the surface due to corrosion. The area on which the mapping was done is presented in Fig. 14B where we can observe the distribution of corroded parts in comparison with C38 Steel area the entire plate was completely attacked by the acid.

Figure 14C shows an extrapolation of the mapping area over the entire plate carried out with Horiba's Labspec 6 software, which makes it possible to show the more general distribution throughout the plate and highlight the coordinated areas in comparison with the C38 steel zone.

For Raman mapping of a parts of Carbon Steel plate C38 in HCl 1M for 4 h immersion, the first pick at 1380 cm^{-1} will be presented in red to show the corroded part and the second pick at 1580 cm^{-1} relating to the presence of terpenes on the surface is represented in blue to show the inhibited part.

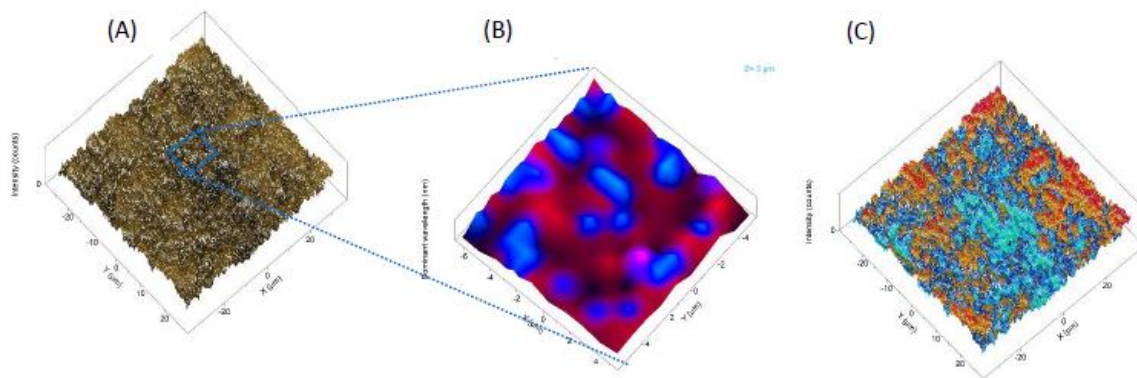


Fig. 14 – 3D Electronical microscopy morphologies (A) and Raman mapping of a parts of Carbon Steel plate C38 in HCl 1M for 4 h immersion (B) and Labspec 6 Mapping Extrapolation in all Carbon Steel plate C38 in HCl 1M (C).

Figure 15d shows the 3D image of the plate in an acidic 1M HCl medium with 100 ppm *Mentha Pulegium* Essential Oil, where we can notice an irregularity in the surface due to corrosion and inhibited parts due to the presence of *Pulegium* Essential Oil. The area on which the mapping was done is presented in Fig. 15e where we can observe the distribution of corroded parts in comparison with non-corroded parts. The plate

shows a reversal of the corrosion process with the majority presence of the blue part representing the inhibited part.

Figure 15f shows an extrapolation of the mapping area over the entire plate carried out with Horiba's LabSpec 6 software, which makes it possible to show the more general distribution throughout the plate and highlight the inhibited areas in comparison with the corroded zones.

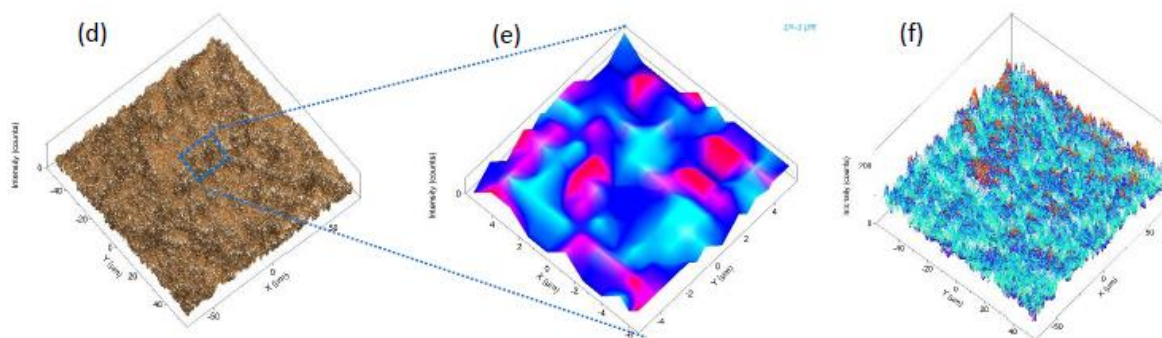


Fig. 15 – 3D Electronical microscopy morphologies (d) and Raman mapping of a parts of Carbon Steel plate C38 in HCl 1M + 100 ppm *Mentha Pulegium* Essential Oil for 4 h immersion (e) and Labspec 6 Mapping Extrapolation in all Carbon Steel plate C38 in HCl 1M+ 100 ppm *Mentha Pulegium* Essential Oil for 4 h immersion (f).

The Raman results furnish indisputable evidence of *Mentha Pulegium* Essential Oil adsorption onto the steel surface. This robustly validates the model proposing the obstruction of active sites, effectively preventing easy corrosion of the steel.

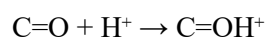
Explanation of the proposed inhibition mechanism

In the presence of an acidic medium (HCl), carbon steel is subjected to corrosive attack due to the presence of H^+ and Cl^- ions that promote the

dissolution of iron (Fe), thus weakening the metal structure.

The chloride ions Cl^- present in the corrosive solution can adsorb onto the positively charged metal surface due to electrostatic interactions.

When the inhibitor is introduced into this medium (Fig. 17), the molecules of its main component « pulegone » can interact with the metal surface through the carbonyl group ($C=O$) present in its structure. This leads to the protonation of oxygen, which becomes positively charged and makes pulegone more electrophilic.⁶⁶



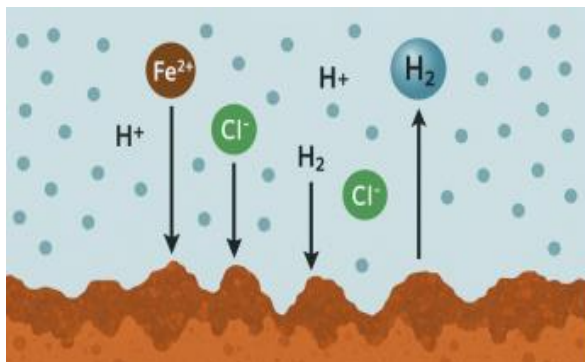


Fig. 16 – Deterioration of metal surface.

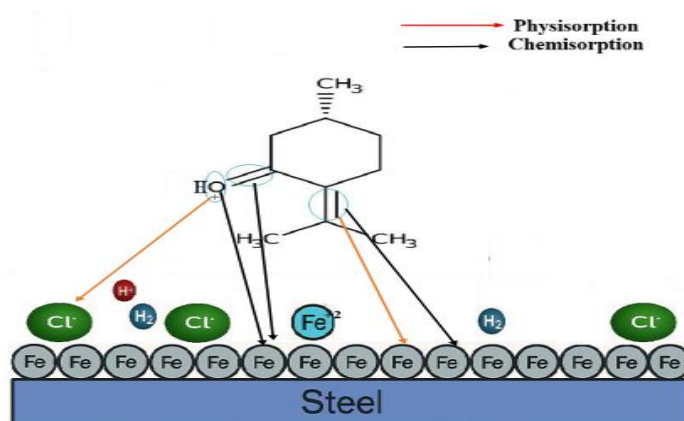


Fig. 17 – Corrosion inhibition mechanism of Carbon steel by Pulegone in HCl medium.

These protonated molecules interact electrostatically with negatively charged chloride ions, specifically adsorbed on the metal surface and the adsorption process occurs by physisorption (represented by a red arrow in the diagram).

Also π bonds (in the C=C double bonds of pulegone) can interact with the d orbitals of iron by Van der Waals forces (π -metal).

In parallel, or in a second step, chemical adsorption can occur, involving the formation of covalent or coordination bonds between pulegone oxygen atoms or its π electrons and iron atoms (Fe^{2+}) present on the steel surface (represented by a black arrow in the diagram).²

Through these chemical and physical interactions, pulegone forms an adsorbed layer on the iron surface. This layer acts as a physical and electrostatic barrier, preventing corrosive ions such as Cl^- and H^+ from reaching the metal.

CONCLUSION

The primary aim of this study is to investigate the corrosion inhibition of C38 steel in a harsh 1M hydrochloric acid environment using the essential

oil derived from the *Mentha pulegium* plant. The investigation employs both the gravimetric method and surface treatment through Raman spectroscopy.

Upon analyzing the obtained results, several conclusions can be drawn. Firstly, the aerial parts of the *Mentha pulegium* plant emerge as a promising green inhibitor source for combating steel corrosion in hydrochloric acid. Secondly, the inhibition rate of *Mentha pulegium* oil (MP oil) demonstrates an upward trend with increasing extract concentration, reaching a peak of 63% at 100 ppm, but decreases as the temperature within the 30–60°C range rises. Thirdly, M.P.E.O and its primary compound, pulegone, exhibit moderate inhibitory effects on C38 corrosion in a 1M HCl solution, with the addition of KI enhancing inhibition performance.

Furthermore, the degree of synergism decreases with increasing experimental temperature, and the values of synergism parameter (SP) are consistently less than unity. The adsorption of the inhibitor on the steel surface in acidic medium, both in the absence and presence of KI, conforms to the Langmuir adsorption isotherm. This model implies that corrosion inhibition arises from the formation of a monolayer on the metal surface, restricting electrolyte access, with negligible interactions

between the adsorbed particles. The presence of KI contributes to increased adsorption of the inhibitor.

The thermodynamic data derived from the adsorption isotherms reveal a physically adsorbed inhibitor at the metal interface in the studied medium.

Lastly, Raman mapping analysis is supplying information pertaining to the distribution of corroded and inhibited parts for carbon steel samples in acidic medium with and without the presence of inhibitor and hence is a potential technique for assessing the effectiveness and genuineness of corrosion inhibition.

Overall, these findings shed light on the effectiveness of *Mentha Pulegium* essential oil as a corrosion inhibitor in challenging acidic conditions, showcasing potential applications in corrosion control strategies.

REFERENCES

1. A. Batah, A. H. Al-Moubaraki and E. A. Noor, *J. Coatings.*, **2024**, *14*, 77.
2. S. M. Lashgari, G. Bahlakeh and B. Ramezanzadeh, *J. Mol. Liq.*, **2021**, *335*, 115897.
3. J. E. Bringas, "Handbook of Comparative World Steel Standards", 3rd ed., ASTM International, 2004.
4. T. D. Manh, T. L. Huynh, B. V. Thi, S. Lee, J. Yi and N. N. Dang, *J. ACS. Omega.*, **2022**, *7*, 8874–8886.
5. C. Verma, E. E. Ebenso, I. Bahadur, and M. A. Quraishi, *J. Mol. Liq.*, **2018**, *266*, 577–590.
6. M. Faiz, A. Zahari, K. Awang and H. Hussin, *J. RSC. Adv.*, **2020**, *10*, 6547.
7. S. Saravanamoorthy and S. Velmathi, *J. Prog. Org. Coat.*, **2013**, *76*, 1527–1535.
8. D. K. Verma and F. Khan, *J. Res. Chem. Intermed.*, **2016**, *42*, 3489–3506.
9. A. Ansari, Y. Youssefi, M. Tanghourte, N. Ouassou, N. Asoufar, M. Znini, H. Lgaz, E. H. Mabrouk, M. Azrou and H. S. Lee, *J. Coatings.*, **2024**, *14*, 1164.
10. I. B. Obot, D. D. Macdonald and Z. M. Gasem, *J. Corros. Sci.*, **2015**, *99*, 1–30.
11. R. L. C. Mendoza, E. G. Moreno, E. G. Percástegui, E. A. Torres, J. C. Borbolla, J. A. R. Avila, J. G. A. Rodríguez, O. O. Neria, P. Thangarasu and J. L. Franco, *J. Chem. Inf. Model.*, **2015**, *55*, 2391.
12. A. Rubaye, A. Abdulwahid, S. B. AlBaghdadi, A. AlAmiery, A. Kadhum and A. Mohamad, *Int. J. Electrochem. Sci.*, **2015**, *10*, 8200–8209.
13. A. Michael, A. Irene, "Handbook of Corrosion Inhibitors", 2nd ed, Synapse Information Resources Inc, 2001.
14. M. B. Pial and M. A. Islam, *J. Results Surfs. Interfaces.*, **2025**, *19*, 100516.
15. M. Bathily, K. Cissé, Y. Youssefi, O. Omar, L. Oucheikh, B. Ngom, M. Znini, D. Gassama and M. Jean Costa, *J. Chem.*, **2024**, *12*, 1596–1620.
16. M. Bathily, K. Cissé, Y. Youssefi, O. Omar, L. Oucheikh, B. Ngom, M. Znini, D. Gassama and M. Jean Costa, *J. Anal. Bioanal. Electrochem.*, **2023**, *15*, 891–913.
17. A. M. Abdel-Gaber, B. A. Abd-El-Nabey, I. M. Sidahmed, A. M. El Zayady and M. Saadawy, *J. Corros. Sci.*, **2006**, *48*, 2765.
18. B. S. Mahdi, M. K. Abbass, M. K. Mohsin, W. K. Al azzawi, M. M. Hanoon, M. H. H. Al kaabi, L. M. Shaker, A. A. Alamiery, W.N. R. W Isahak and A. A. H. Kadhum, *J. Molecules.*, **2022**, *27*, 4857.
19. R. Ihamdane, M. Tiskar, B. Outemsa, L. Zelmat, O. Dagdag, A. Berisha, E. Berdimurodov, E. E. Ebenso and A. Chaouch, *J. Arab For Sci And Eng.*, **2023**, *48*, 7685–7701.
20. A. Zaher, L. Hassane, A. Boukhraz, A. Aldalbahi, H. Lee, B. Bourkhiss and M. Ouhssine, *J.Coatings.*, **2024**, *14*, 1556.
21. E. F. Olasehinde, S. J. Olusegun, A.S. Adesina, S. A. Omogbehin and H. M. Yahayah, *J. Nat. Sci.*, **2013**, *11*, 83–90.
22. O. Benali, S. Chaouki and R. Salghi, *J. Res. Chem. Intermed.*, **2014**, *40*, 259–268.
23. H. Cang, F. Zhenghao, H. Xiao, J. Huang and Qi. Xu, *Int. J. Electrochem. Sci.*, **2012**, *7*, 8869–8882.
24. X. Li, S. Deng and H. Fu, *Corros. Sci.*, **2012**, *62*, 163–175.
25. S. N. Victoria, R. Prasad and R. Manivannan, *Int. J. Electrochem. Sci.*, **2015**, *10*, 2220–2238.
26. R. Karthik, P. Muthukrishnan, S. Chen, B. Jeyaprabha and P. Prakash, *Int. J. Electrochem. Sci.*, **2015**, *10*, 3707–3725.
27. K. K. Anupama and J. Abraham., *J. Res. Chem. Intermed.*, **2013**, *39*, 4067–4080.
28. L. Y. S. Helen, A. A. Rahim, B. Saad, M. I. Saleh and P. B. Raj, *Int. J. Electrochem. Sci.*, **2014**, *9*, 830–846.
29. M. Chevalier, F. Robert, N. Amusant, M. Traisnel, C. Roos and M. Lebrini, *J. Electrochim. Acta.*, **2014**, *31*, 96–105.
30. G. Ji, P. Dwivedi, S. Sundaram and R. Prakash, *J. Ind. Eng. Chem. Res.*, **2013**, *52*, 10673–10681. 23. B. Pushpanjali, A. R. Suma and R. padmalatha, *Int. J. Innov. Res. Sci. Eng. Technol.*, **2015**, *4*, 325 – 333.
31. M. M. Ihebroke, C. M. Nwandu, B. O. Kelechukwu and E. E. Oguzie, *J. Proceedia mater. Sci.*, **2014**, *5*, 222–231.
32. S. V. Priya, *Int. J. Adv. Res. Chem. Eng.*, **2016**, *1*, 41–47.
33. P. Kalaiselvi, S. Chellammal, S. Palanichamy and G. Subramanian, *J. Mater. Chem. Phys.*, **2010**, *120*, 643–648.
34. A. Ostovari, S. M. Hoseinie, M. Peikari, S. R. Shadizadeh and S. J. Hashemi, *J. Corros. Sci.*, **2009**, *51*, 1935–1949.
35. M. H. Hussin and M. J. Kassim, *J. Mater. Chem. Phys.*, **2011**, *125*, 461–468.
36. M. A. Quraishi, A. Singh, V. K. Singh, D. K. Yadav and A. K. Singh, *J. Mater. Chem. Phys.*, **2010**, *122*, 114–122.
37. M. Abdallah, A. Fawzy, H. Hawsawi, R. S. A. Hameed and S. S. AlJuaid, *Int. J. Electrochem. Sci.*, **2020**, *15*, 8129–8144.
38. M. Lebrini, F. Robert, A. Lecante and C. Roos, *J. Corros. Sci.*, **2011**, *53*, 687–695.
39. I. A. Kartsonakis and C. A. Charitidis, *J. Appl. Sci.*, **2020**, *10*, 6594.
40. H. P. Dias, E. V. Barros, C. Sad, E. R. Yapuchura, A. O. Gomes, R. Moura and W. Romao, *J. Braz. Chem. Soc.*, **2018**, *29*, 1690–1700.
41. D. R. Veys, S. Reguer, L. G. Bellot, F. Mirambet and E. Rocca, *J. Corros. Sci.*, **2018**, *136*, 1–8.
42. F. S. de Souza and A. Spinelli, *J. Corros. Sci.*, **2009**, *51*, 642–649.
43. X. Nie, X. Li, C. Du, Y. Huang and H. Du, *J. Raman. Spectrosc.*, **2009**, *40*, 76–79.
44. N. Chabane, F. Dergal, T. Attar, N. Belarbi, I. Chikhi, S. Cherigui and K. Bachari, *Rev. Roum. Chim.*, **2023**, *68*, 371–381.

45. N. Belarbi, F. Dergal, I. Chikhi, D. Lerari, B. Dahmani, N. Choukchou Braham and K. Bachari, *J. Chem.Chem. Technol.*, **2023**, *17*, 7–17.
46. N. Belarbi, F. Dergal, I. A. El Hassi, T. Attar, D. lerari, B. Dahmani and K. Bachari, *J. Anal. Bioanal. Electrochem.*, **2021**, *13*, 340–357.
47. N. Belarbi, F. Dergal, I. Chikhi, S. Merah, D. Lerari and K. Bachari, *Int. J. Ind. Chem.*, **2018**, *9*, 115–125.
48. F. Brahmi, N. K. Khodja, R. Bezeghouche, S. Bouharis, M. F. Elsebai, K. Madani and L. B. Makhlof, *Jordan J. Pharm. Sci.*, **2023**, *16*, 268–281.
49. F. Z. Benomari, V. Andreu, J. Kotarba, M. E. A. Dib, C. Bertrand, A. Muselli, J. Costa and N. Djabou, *Environ. Sci. Pollut. Res.*, **2018**, *25*, 29889–29900.
50. I. Telci, I. Demirtas, E. Bayram, O. Arabaci and O. Kacar, *J. Ind. Crops. Prod.*, **2010**, *32*, 588–592.
51. B. S. Mahdi, M. K. Abbass, M. K. Mohsin, W. K. Alazzawi, M. M. Hanoon, M. H. H. Al kaabi, L. M. Shaker, A. A. Alamiery, W. N. R. W. Isahak and A. A. H. Kadhum, *J. Molecules.*, **2022**, *27*, 4857.
52. E. E. Oguzie, C. Unaegbu, C. N. Ogukwea, B. N. Okolue and A. I. Onuchuku, *J. Mater. Chem. Phys.*, **2004**, *84*, 363–368.
53. X. Li, S. Deng and H. Fu, *J. Corros. Sci.*, **2010**, *52*, 3413–3420.
54. M. V. Fiori-Bimbi, P. E. Alvarez, H. Vaca and C. A. Gervasi, *J. Corros. Sci.*, **2015**, *92*, 192–199.
55. O. A. Akinbulumo, O. J. Odejebi and E. L. Odekanle, *J. Results. Mater.*, **2020**, *5*, 100074.
56. M. Erna, H. Herdini and D. Futra, *Int. J. Chem. Engg.*, **2019**, *32*, 85141.
57. S. C. Ikpeseni, G. O. Odu, H. I. Owamah, P. U. Onochie and D. C. Ukala, *Arab.J.Sci.Eng.*, **2021**.
58. K. S. Sudhish and E. E. Eno, *Int. J. Electrochem. Sci.*, **2011**, 3277–3291.
59. K. Okorosaye-Orubite, I. R. Jack, M. Ochei and O. J. Akaranta, *J. Appl. Sci. Environ. Manage.*, **2007**, *11*, 27–31.
60. A. Ishtiaque, P. Rajendra and M. A. Quraishi, *J. Solid. State. Electrochem.*, **2010**, *14*, 2095–2105.
61. X. H. Li, S. D. Deng and H. Fu, *J. Corros. Sci.*, **2009**, *51*, 1344–1355.
62. X. Li, S. Deng and H. Fu, *J. Corros. Sci.*, **2010**, *52*, 3413–3420.
63. F. Bentiss, M. Lebrini and M. Lagréné, *J. Corros. Sci.*, **2005**, *47*, 2915–2931.
64. W. H. Li, Q. He, S. T. Zhang, C. L. Pei and B. R. Hou, *J. Appl. Electrochem.*, **2008**, *38*, 289–295.
65. E. Bensajjay, S. Alehyen, M. El Achouri and S. Kertit, *J. Anti. Corros. Meth. Mater.*, **2003**, *50*, 402–409.
66. H. L. Monteiro, A. F. Ribeiro, M. J. C. Modesto, E. H. A. Andrade, J. A. S. Souza, J. Nero, A. F. S. Rente, R. D. Noce, J. P. I. de Souza, C. A. B. da Silva, M. V. S. Paula, and A. A. B. Maia, *J. ACS Omega.*, **2024**, *9*, 45348–45357.
67. K. Aramaki, M. Hagiwara and H. Nishihara, *J. Electrochem. Soc.*, **1987**, *134*, 1896–1901.
68. K. Aramaki, M. Hagiwara and H. Nishihara, *J. Corros. Sci.*, **1987**, *27*, 487–497.
69. T. A. Mouheddin, A. U. Saviour, B. O. Ime and A. A. Shaikh, *J. RSC. Adv.*, **2018**, *8*, 1764–1777.
70. Z. Bensouda, E. H. El Assiri, M. Sfaira, M. E. Touhami, A. Farah and B. Hammouti, *J. Bio. Tribo. Corros*, **2019**, *5*, 84.
71. N. Mechbal, M. Bouhrim, M. Bnouham, B. Hammouti, Y. Karzazi, S. Kaya and G. Serdaroğlu, *J.Mol. Liquids.*, **2021**, *331*, 115771.
72. K. Boumhara, M. Tabyaoui, C. Jama and F. Bentiss, *J. Ind. Eng. Chem.*, **2015**, *29*, 146–155.

